# Gravitational waves from dark domain walls

Ø. Christiansen<sup>1,3</sup> \*, J. Adamek<sup>2</sup> \*\*, F. Hassani<sup>1</sup> \*\*\*, and D. Mota<sup>1</sup> \*\*\*\*,

#### **ABSTRACT**

For most of cosmic history, the evolution of our Universe has been governed by the physics of a 'dark sector', consisting of dark matter and dark energy, whose properties are only understood in a schematic way. The influence of these constituents is mediated exclusively by the force of gravity, meaning that insight into their nature must be gleaned from gravitational phenomena. The advent of gravitational-wave astronomy has revolutionised the field of black hole astrophysics, and opens a new window of discovery for cosmological sources. Relevant examples include topological defects, such as domain walls or cosmic strings, which are remnants of a phase transition. Here we present the first simulations of cosmic structure formation in which the dynamics of the dark sector introduces domain walls as a source of stochastic gravitational waves in the late Universe. We study in detail how the spectrum of gravitational waves is affected by the properties of the model, and extrapolate the results to scales relevant to the recent evidence for a stochastic gravitational wave background. Our relativistic implementation of the field dynamics paves the way for optimal use of the next generation of gravitational experiments to unravel the dark sector.

**Key words.** N-body simulation – dark energy – domain walls – gravitational waves – gravity

For most of cosmic history, the evolution of our Universe has be matter and dark energy, whose properties are only understood in exclusively by the force of gravity, meaning that insight into their of gravitational-wave astronomy has revolutionised the field of bl cosmological sources. Relevant examples include topological def of a phase transition. Here we present the first simulations of cos introduces domain walls as a source of stochastic gravitational wave background. Our relativistic impleme next generation of gravitational experiments to unravel the dark se **Key words**. *N*-body simulation – dark energy – domain walls – g **1. Introduction**The detection of the nanohertz stochastic gravitational wave background by the pulsar timing arrays (Agazie et al. 2023; Antoniadis et al. 2023; Reardon et al. 2023; Xu et al. 2023) opens a new window for studying gravitational systems at cosmological scales. The signal observed by the NANOGrav array (Agazie et al. 2023) consists of correlated timing residuals of 68 millisectial scales. The signal observed by the haracteristic strain of the stochastic gravitational wave background (Maiorano et al. 2021), i.e. the characteristic fractional change in the length of a hypothetical detector arm. An astrophysical background from supermassive black hole inspirals is predicted (Phinney 2001) to yield  $h_c \sim f^{-2/3}$  and hence a spectrum of timing residuals that tilts as  $f^{-13/3}$ . While supermassive black holes remain a viable explanation of the observed signal, a tilt between  $f^{-2.6}$  and  $f^{-3.8}$  is preferred by the data, which is in mild tension with the prediction. This has prompted a large number of investigations into alternative explanations, exploring possible phenomena in the dark second content of the content This has prompted a large number of investigations into alternative explanations, exploring possible phenomena in the dark sector or in the early Universe (Agazie et al. 2023; Babichev

One hypothetical source of gravitational waves are topological defects that are generically produced at certain types of phase transitions. Depending on the nature of the spontaneously broken symmetry, the defects can take the form of cosmic strings or domain walls (Kibble 1976; Saikawa 2017; Vilenkin 1985; Vachaspati 2007). In particular, if the vacuum manifold splits

into two (or more) isolated points, domain walls separate the regions that have settled into different vacua during the phase transition. The case where the phase transition happens in the early Universe at a high energy scale has been studied thoroughly in the recent literature (Ramazanov et al. 2022; Blasi et al. 2023; Li 2023; Babichev et al. 2023; Kitajima et al. 2023a; Gouttenoire & Vitagliano 2023; Kitajima et al. 2023b), owing to the dimensional argument that frequencies in the nanohertz range today correspond to the size of the causal horizon (the scale that sets the typical size of different vacuum domains) when the Universe had a temperature of several trillion degrees Kelvin.

In this work instead, we consider domain walls appearing in the late-time Universe due to phase transitions in the dark energy field. This scenario has not yet been studied in the context of stochastic gravitational waves. We consider the (a)symmetron model (Perivolaropoulos & Skara 2022), a generalisation of the symmetron (Hinterbichler & Khoury 2010; Hinterbichler et al. 2011), a theory of gravity with an extra scalar degree of freedom. Such extra degrees of freedom are a general prediction of physics beyond the Standard Model (Clifton et al. 2012). The symmetron can be regarded as a generic scalar effective field theory (EFT), with a potential parameterized as a quartic-order Taylor polynomial around the field origin. The quartic self-coupling term is chosen to be positive so that the potential is bounded from below, while the quadratic term is chosen to be negative in order to have a Higgs-like phase transition. The  $\mathbb{Z}_2$  symmetry protects against large quantum corrections (Hinterbichler & Khoury 2010). The symmetron has a universal coupling to the matter sector through a conformal factor, which adds a coupling term to the effective mass of the scalar field. The model can thus be seen as a typical EFT limit for  $\mathbb{Z}_2$  symmetric Horndeski theories in the case where the field  $\phi/M_{\rm pl}$  is small so that the Taylor expansion can

<sup>&</sup>lt;sup>1</sup> Institute of Theoretical Astrophysics, University of Oslo, Sem Sælands vei 13, 0371 Oslo, Norway

<sup>&</sup>lt;sup>2</sup> Institut für Astrophysik, Universität Zürich, Winterthurerstrasse 190, 8057 Zürich, Switzerland

<sup>&</sup>lt;sup>3</sup> CEICO, Institute of Physics of the Czech Academy of Sciences, Na Slovance 1999/2, 182 00, Prague 8, Czechia

<sup>\*</sup> oyvinch@fzu.cz

julian.adamek@uzh.ch

farbod.hassani@astro.uio.no

<sup>\*\*\*\*</sup> d.f.mota@astro.uio.no

be truncated. In addition, we have added an odd term to the potential that explicitly breaks the  $\mathbb{Z}_2$  symmetry, so that we can study the case where the vacuum degeneracy is lifted and one of the minima is favoured.

The universal coupling to the matter sector mediates a fifth force that affects cosmological structure formation and is tightly constrained by local gravity experiments (Will 2014; Bertotti et al. 2003; Esposito-Farese 2004; Burrage et al. 2023; Llinares & Brax 2019). When the local matter density falls below some critical threshold  $\rho_*$ , it triggers the  $\mathbb{Z}_2$  phase transition, and the field settles into either of two minima. A crucial difference from the early Universe is that the late-time Universe has very large fluctuations in the local density, so that the phase transition happens in different places at different times. The resulting domains are separated by domain walls that are moulded by the sheets and filaments in the cosmic large-scale structure. This way, a large number of domain walls can be formed in a Hubble volume. Both their energy density and Compton scale are free parameters, but the former is often chosen well below the critical density such that the expansion rate of the Universe is not affected significantly. However, they can still produce a considerable stochastic gravitational wave signal if their time evolution is violent enough. In the case where the potential is not symmetric, the asymmetry tends to destabilise the domains that occupy the higher minimum. Spontaneous reconfiguration of domains then leads to the collision and annihilation of domain walls, adding a further source of gravitational waves that is qualitatively different from stable domain walls.

In addition to being considered as a model for dark matter (Burrage et al. 2019; Käding 2023), the symmetron can also be motivated by the recent results of the Dark Energy Spectroscopic Instrument (DESI), which hint at a dynamical source for late-time cosmic acceleration (DESI Collaboration et al. 2024). In recent work (Christiansen et al. 2025) it was shown that a consistent evolution of the cosmic acceleration can be found using the symmetron together with a degravitation mechanism. Alternatively, one can still imagine obtaining a consistent accelerated expansion from the combination of the slow-rolling scalar with decreasing potential energy (and equation of state parameter  $w \sim -1$ ) and the increasingly dominant domain walls  $(w \sim -2/3)$ . The symmetron has also been linked to the detection of an anomalous Integrated Sachs-Wolfe (ISW) signal (Christiansen et al. 2024; Kovács et al. 2019), and to claims of large structure being in tension with the cosmological principle (Secrest et al. 2021, 2022; Peebles 2023; Lopez et al. 2024; Nadathur 2013).

# 2. Gravitational wave spectra

We write the space-time line element of the expanding Friedmann universe with linearised gravitational waves as

$$ds^2 = a^2(\tau) \left[ -c^2 d\tau^2 + \left( \delta_{ij} + h_{ij} \right) dx^i dx^j \right], \tag{1}$$

where a denotes the scale factor, c is the speed of light,  $d\tau = a^{-1}dt$  is a conformal time element,  $x^i$  are comoving Cartesian coordinates on the spatial hypersurface, and  $h_{ij}$  is the transverse and traceless tensor perturbation containing the gravitational waves. A sum is implied over repeated indices. Our simulations also track scalar and vector perturbations of the metric (Adamek et al. 2016a), but these are relevant mainly for matter dynamics and shall be omitted in the following discussion for brevity. In Fourier space, the tensor perturbations obey a damped

oscillator equation that is driven by the spin-2 projection of the stress-energy tensor (Adamek et al. 2016b),

$$\ddot{\tilde{h}}_{ij} + 2\mathcal{H}\dot{\tilde{h}}_{ij} + c^2 k^2 \tilde{h}_{ij} = \frac{16\pi G}{c^2} \left( P_i^l P_j^m - \frac{1}{2} P_{ij} P^{lm} \right) \tilde{T}_{lm} \,, \tag{2}$$

where a dot denotes a derivative with respect to  $\tau$ ,  $\mathcal{H} = d \ln a/d\tau$  is the conformal Hubble rate, G is Newton's gravitational constant, k is the comoving Fourier wavenumber, and  $P_{ij} = \delta_{ij} - k^{-2}k_ik_j$  is a transverse projector. A tilde indicates spatial Fourier transform, and  $\tilde{T}_{lm}$  is the spatial part of the stress-energy tensor in Fourier space.

In our numerical simulations, we compute the stress-energy tensor of the scalar field, and hence of the domain walls, non-perturbatively by solving the full equations of motion discretised on a three-dimensional grid. The stress-energy is taken to Fourier space, using fast Fourier transforms, to source the wave equation (2) that we integrate separately for each wave vector using a temporal leapfrog integrator. We evolve only the Fourier components for which our time stepping guarantees a stable integration, which requires  $k \leq (c\Delta\tau)^{-1}$  for an integration step  $\Delta\tau$ . At any point in time, we can estimate the power spectrum  $P_h(k)$  of  $\dot{h}_{ij}$ ,

$$\sum_{i,j} \left\langle \dot{\tilde{h}}_{ij}(\boldsymbol{k},\tau) \dot{\tilde{h}}_{ij}(\boldsymbol{k}',\tau) \right\rangle = \delta_{\mathrm{D}}^{(3)}(\boldsymbol{k}+\boldsymbol{k}') P_{h}(k) , \qquad (3)$$

where  $\delta_{\rm D}^{(3)}$  is the three-dimensional Dirac delta distribution. Assuming that the gravitational waves propagate freely at the time when we perform the measurement, this spatial two-point correlation is directly related to the temporal one via the retarded time. In this case one finds that the spectral density in the frequency domain,  $S_h(f)$ , is simply given by  $2\pi c^3 S_h(f) = P_h(k = 2\pi f/c)$ .

It is common practice to express the spectrum in terms of the energy density of gravitational waves (Allen & Romano 1999),

$$\rho_{\rm gw} = \int_0^\infty \frac{d\rho_{\rm gw}}{df} df = \frac{c^2}{32\pi G} \sum_{i,j} \left\langle \dot{h}_{ij}(\mathbf{x}, \tau) \dot{h}_{ij}(\mathbf{x}, \tau) \right\rangle 
= \frac{\pi c^2}{2G} \int_0^\infty f^2 S_h(f) df . \quad (4)$$

One may furthermore define the dimensionless density per logarithmic frequency interval,

$$\Omega_{\rm gw}(f) = \rho_{\rm crit}^{-1} \frac{d\rho_{\rm gw}}{d\ln f} = \frac{4\pi^2}{3H_0^2} f^3 S_h(f) = \frac{2\pi^2}{3H_0^2} f^2 h_c^2(f),$$
 (5)

where  $H_0$  is the present-day Hubble parameter and the critical density of the Universe is given by  $\rho_{\rm crit} = 3c^2H_0^2/(8\pi G)$ .

# 3. Numerical simulations

The asymmetron model depends on four parameters (Christiansen et al. 2023): the Compton wavelength  $L_C$ , indicating the correlation length of the scalar field in vacuum; the cosmological redshift of the phase transition  $z_*$ , indicating the time when the background matter density is equal to the critical density  $\rho_*$  of the phase transition; the average strength of the fifth force relative to gravity,  $\bar{\beta} = (\beta_+ + \beta_-)/2$ ; and the respective difference  $\Delta\beta = \beta_+ - \beta_-$  in the two minima. The asymmetron reduces to the symmetron for the choice  $\Delta\beta = 0$ , in which case the scalar potential is symmetric.

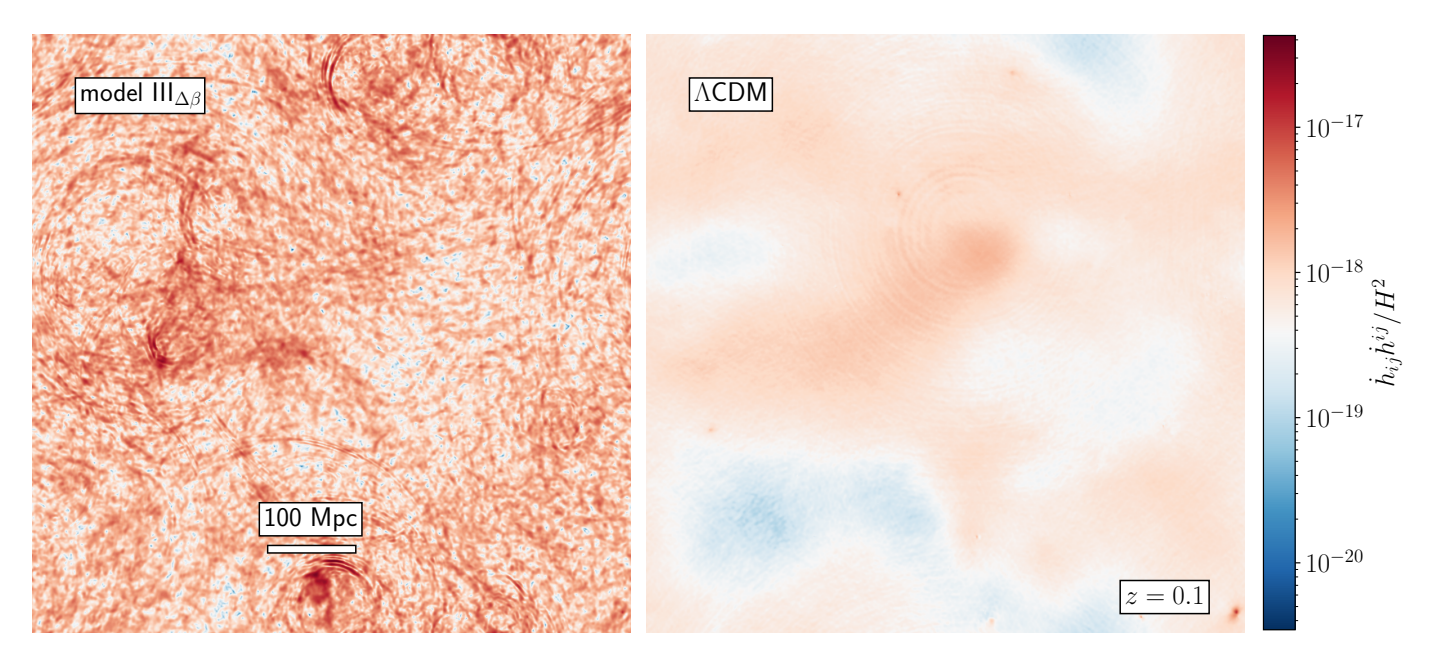


**Fig. 1.** A slice through the simulation volume at redshift z=0.1, showing the tensor wave intensity  $\sum_{i,j}\dot{h}_{ij}^2/H^2$ , where H is the Hubble factor. Model  $III_{\Delta\beta}$ , shown on the left, has the parameters  $(L_C, z_*, \bar{\beta}, \Delta\beta/\bar{\beta}) = (1480 \text{ kpc}, 0.1, 8, 10\%)$ . A standard cosmology without the scalar field is shown on the right. (The Supplementary Material contains animations that show the evolution of the fields and the formation of cosmic structure.)

We run two suites of simulations<sup>1</sup> varying parameters about their respective values in a reference model. Within the first suite, three high-resolution simulations (1280<sup>3</sup> grid points, 742 Mpc box size) are labelled I-III, and two lower-resolution simulations (512<sup>3</sup> grid points, 742 Mpc box size) are labelled IV and V. The five simulations within the second suite roughly match the higher resolution but use a smaller volume (256<sup>3</sup> grid points, 148 Mpc box size), and are labelled i-v. Among the larger volume simulations, the reference model I has parameters  $(L_C, z_*, \bar{\beta}, \Delta\beta) = (1480 \,\text{kpc}, 0.1, 8, 0)$ . Models II-V vary one parameter at a time, using  $L_C = 1111 \,\mathrm{kpc}$ ,  $\Delta \beta/\bar{\beta} = 10\%$ ,  $z_* = 0$ and  $\bar{\beta} = 12$ , respectively. For quick reference, we use a subscript to indicate the parameter that was varied with respect to the reference model. In the smaller volume simulations, our reference model i has  $(L_C, z_*, \bar{\beta}, \Delta\beta) = (743 \text{ kpc}, -0.2, 90, 0)$ , and models ii-v use  $L_C = 801 \,\mathrm{kpc}$ ,  $\Delta \beta/\bar{\beta} = 30\%$ ,  $z_* = -0.13$  and  $\bar{\beta} = 120$ , respectively. The choices of Compton wavelength are close to the resolution limit of these simulations, and we comment more on numerical resolution and convergence in appendix A. Smaller box sizes, allowing correspondingly smaller Compton wavelengths, become increasingly expensive to simulate due to the shorter dynamical timescales involved. The values of  $\beta$ chosen are the largest that satisfy the code's linearisation scheme (Christiansen et al. 2023). The small choices of  $z_* \leq 0$  are largely unconstrained (Burrage et al. 2023).

The left panel of figure 1 shows the intensity of gravitational waves emanating from collapsing domain walls for the model  $\text{III}_{\Delta\beta}$  that has an asymmetry of 10% in the scalar field potential. In contrast, the right panel shows the gravitational wave pattern for a standard  $\Lambda$ -cold-dark-matter ( $\Lambda$ CDM) cosmological model without the scalar field. In this case, the main source of long-wavelength gravitational waves is the evolving large-scale structure.

Figure 2 shows the present-day (z=0) power spectra of gravitational waves, presented in units of dimensionless energy density per logarithmic frequency interval. There is a clear generation of power at the scale corresponding to the Compton wavelength of the theory with a power-law tail extending to lower frequencies. At extremely low frequency, below about  $10^{-16}$  Hz, cosmic large-scale structure (LSS) becomes the dominant source of gravitational waves in most cases. The corresponding amplitude can be predicted from second-order perturbation theory and is indicated as dotted line in the figure, showing good agreement with our simulations in the regime where perturbation theory is valid. The somewhat larger amplitude we find for  $\Lambda$ CDM is due to higher-order nonlinearities and, at the highest wavenumbers, discretisation noise in our numerical scheme.

The following qualitative trends can be seen in our suite of simulations: a smaller Compton wavelength  $L_C$  reduces the amplitude and moves the peak power to a correspondingly smaller scale; a larger average fifth force  $\bar{\beta}$  increases the amplitude; and a later time of symmetry breaking (lower  $z_*$ ) reduces the amplitude and has otherwise a small effect. Finally, adding asymmetry to the potential by choosing  $\Delta\beta>0$ , we find more unstable domains, significantly increasing the contribution of collapsing domain walls to the gravitational wave signal. We find that this component, which consists of a noise of gravitational wave bursts, has a nearly flat spectrum at low frequencies.

The NANOGrav collaboration has presented confidence intervals for the spectral tilt by fitting a power law  $\sim Af^{-\gamma}$  to the timing residuals (Agazie et al. 2023). We measure the spectral tilt  $\gamma$  from our simulations, using the fact that the timing residuals scale as  $\propto \Omega_{\rm gw}f^{-5}$ . Our results are shown in figure 3. We note that all simulations display a plateauing spectral tilt that persists up to the Compton scale. Furthermore, there is no strong indication for a dependence on  $\bar{\beta}$  and  $z_*$ . Stable domain walls seem to generate slightly bluer spectra (lower  $\gamma$ ) compared to the NANOGrav measurement, whereas collapsing and annihilating

<sup>&</sup>lt;sup>1</sup> The code (Christiansen et al. 2024, 2023; Adamek et al. 2016b; Daverio et al. 2016; Llinares & Mota 2013, 2014) is publicly available and can be downloaded at https://github.com/oyvach/AsGRD.

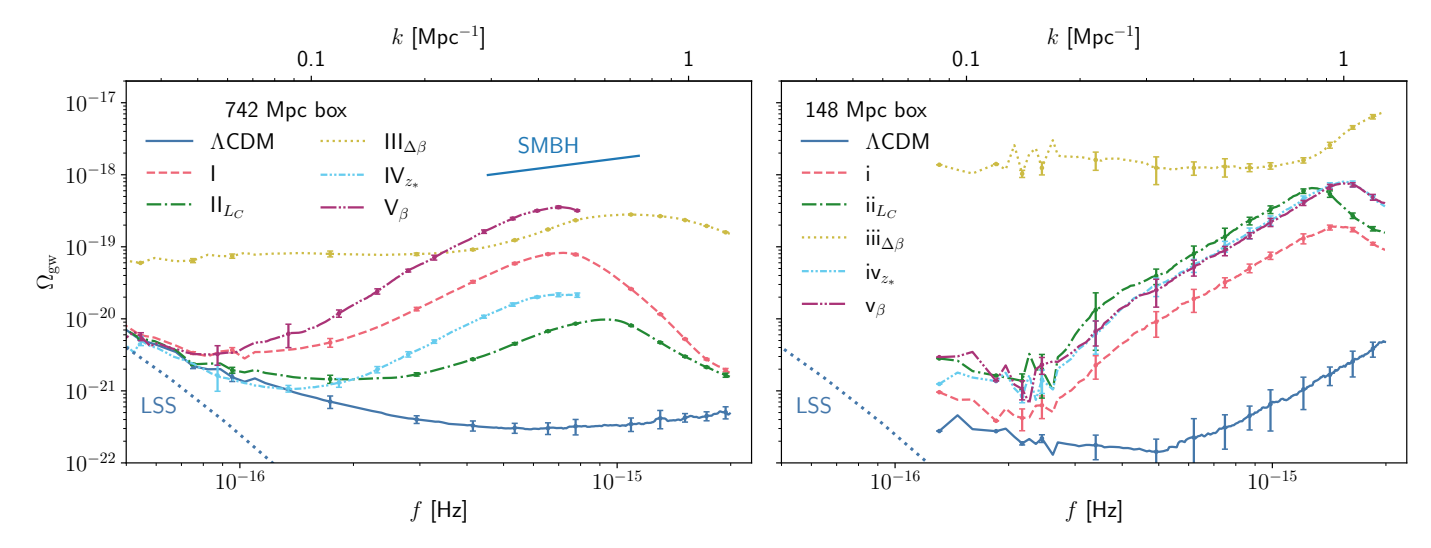


Fig. 2. Power spectra of the time derivative of the tensor perturbation,  $h_{ij}$ , plotted as dimensionless energy density per logarithmic frequency interval. The conversion from Fourier wavenumber k to frequency f assumes the standard dispersion relation  $k = 2\pi f/c$ . Results from the simulations in the larger volume,  $(742 \, \text{Mpc})^3$ , are shown in the left panel and the ones for the smaller volume,  $(148 \, \text{Mpc})^3$ , are shown in the right panel. The error bars indicate the 95% confidence intervals estimated from statistical fluctuations measured for each realisation within a narrow frequency band. The dotted line labelled "LSS" shows the gravitational wave contribution from the evolution of large-scale structure as predicted by second-order perturbation theory. The short blue line labelled "SMBH", inserted as a visual guide only, indicates the expected slope for an astrophysical signal produced by supermassive black hole inspirals. This signal would however appear at very different frequencies and amplitudes.

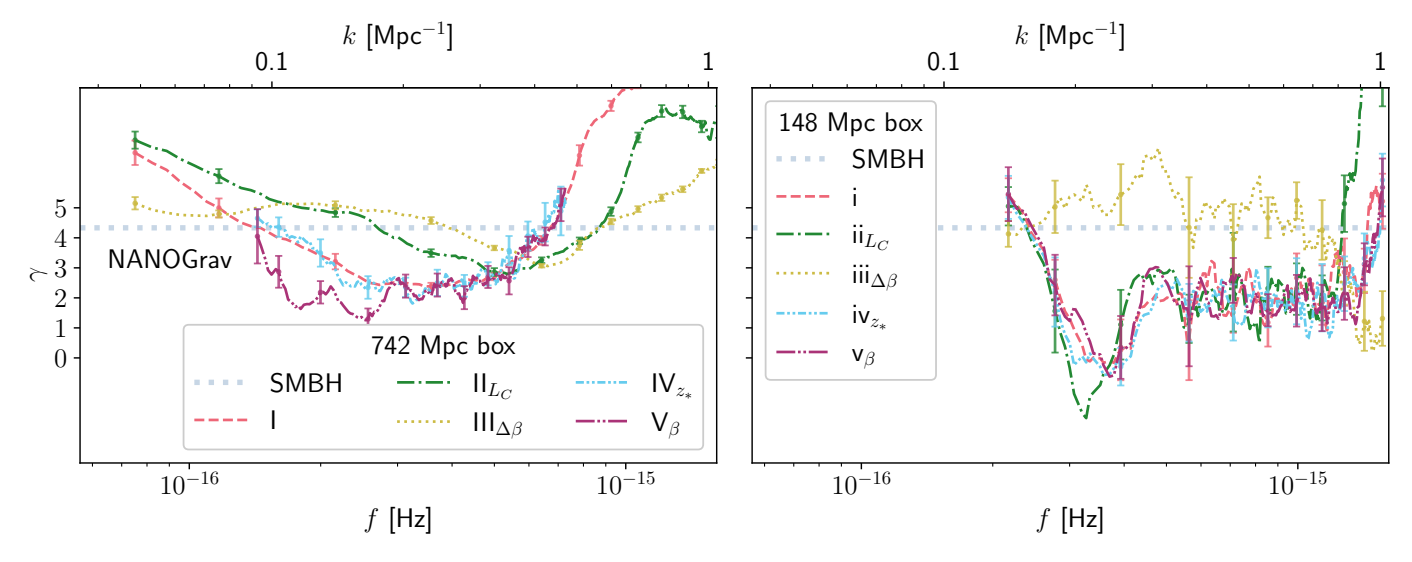


Fig. 3. The spectral index  $\gamma$  inferred from the power spectra shown in figure 2, with error bars indicating 95% confidence intervals. The blue bands show the 68% and 95% confidence intervals reported for the NANOGrav observations that were however taken at much higher frequencies. The dotted horizontal line labelled SMBH indicates the expected spectral index for supermassive black hole inspirals, which would also appear at much higher frequencies.

domain walls (models with  $\Delta\beta > 0$ ) push the tilt all the way to the red side of the NANOGrav posterior.

# 4. Discussion

To connect our results with the NANOGrav measurements, we need to extrapolate eight orders of magnitude towards smaller scales and about ten orders of magnitude in energy density  $\Omega_{\rm gw}$ . Such a huge extrapolation in parameter space comes with several caveats that we address partially, and they should be investigated further in the future. To get some analytic insight, it is useful to consider that, when viewed on scales larger than the thickness of the domain wall, its stress-energy is simply proportional to the

surface tension

$$\sigma \simeq \int_{\phi_{-}}^{\phi_{+}} \sqrt{2V_{\text{eff}}(\phi) - 2V_{\text{eff}}(\phi_{\pm})}, \tag{6}$$

where one integrates between the two asymptotic vacuum values  $\phi_{\pm}$  on the two sides of the wall. At vanishing matter density we have  $\sigma=12\sqrt{2}\,\Omega_{\rm m}^2H_0^4\bar{\beta}^2(1+z_*)^6L_C^3$ . This sets the strength of the gravitational wave source and we expect that  $\Omega_{\rm gw}\propto\sigma^2$ . Our simulations indeed confirm this scaling with  $\bar{\beta}$ , while we find a slightly stronger-than-expected dependence  $\Omega_{\rm gw}\sim(1+z_*)^{14}$ . The dependence on  $L_C$  seems much more complicated than the naive consideration of  $\sigma$  suggests. This may be due to the fact

that domain walls tend to be aligned with sheets and filaments of dark matter, affecting the effective potential and hence the surface tension in a non-trivial way. We point out that the Compton scale  $L_C$  sets the typical length scale over which the field can respond to local variations in the matter density.

Given that  $L_C$  would need to be reduced by some eight orders of magnitude from our reference simulations to reach NANOGrav frequencies, it is difficult to predict the amplitude robustly. The trends seen in our simulations suggest that the amplitude would need to be boosted significantly to reach NANOGrav levels, which can be achieved by increasing  $\bar{\beta}$  or  $z_*$ , or both, presumably by many orders of magnitude. This would yield a model with a very strong fifth force that is however also strongly screened. Allowing for asymmetry in the potential ( $\Delta\beta > 0$ ) is an interesting scenario to explore, as we have seen that the gravitational wave amplitude from collapsing domain walls can easily dominate the signal.

In conclusion, we have shown that a late-time cosmological source may be a viable candidate for providing the observed spectral tilt of the NANOGrav experiment, although matching the signal amplitude remains an open question that requires a significant extrapolation of our results. Nevertheless, this work presents for the first time a full simulation of an ultra-light scalar field in a late-time cosmological N-body code, including a consistent treatment of gravity and sourcing of gravitational waves. Our code provides a new framework and opens the door to studies of the late-time production of gravitational waves from cosmological sources, such as topological defects, late-time phase transitions, and their interaction with structure formation. This tool is set to play an important role at the interface between cosmological surveys and gravitational-wave astronomy, both of which are needed to probe the dark sector and advance our understanding of the nature of gravity.

## Acknowledgements

Ø.C. thanks Constantinos Skordis and the Central European Institute of Cosmology (CEICO) for hosting him during the work on the project. J.A. acknowledges support from the Swiss National Science Foundation. This work was co-funded by the European Union and supported by the Czech Ministry of Education, Youth and Sports (Project No. FORTE – CZ.02.01.01/00/22\_008/0004632). We thank the Research Council of Norway for their support. The simulations were performed on resources provided by UNINETT Sigma2 – the National Infrastructure for High Performance Computing and Data Storage in Norway. This work is supported by a grant from the Swiss National Supercomputing Centre (CSCS) under project ID s1051.

# Author contributions

Ø.C. implemented the model in the code, ran the simulations and did most of the analysis. J.A. proposed and contributed to the code to obtain the gravitational wave signal, and played a leading role in the theoretical interpretation of the results. All authors discussed the results and contributed to the writing.

### Materials & Correspondence

Correspondence and requests for materials should be directed to Øyvind Christiansen (oyvind.christiansen@astro.uio.no).

#### Data availability statement

The data used for producing the figures are available at the link https://zenodo.org/records/10495599.

### Code availability statement

The code 'AsGRD' used to produce the results is available from the maintained repository https://github.com/oyvach/AsGRD. The version of the code used in this paper, along with the post-processing tools, may be found at the link https://zenodo.org/records/10495599.

### References

- Adamek, J., Daverio, D., Durrer, R., & Kunz, M. 2016a, Nature Physics, 12, 346, number: 4 Publisher: Nature Publishing Group
- Adamek, J., Daverio, D., Durrer, R., & Kunz, M. 2016b, Journal of Cosmology and Astroparticle Physics, 2016, 053, arXiv: 1604.06065
- Agazie, G., Anumarlapudi, A., Archibald, A. M., et al. 2023, The Astrophysical Journal, 951, L8, publisher: IOP ADS Bibcode: 2023ApJ...951L...8A
- Allen, B. & Romano, J. D. 1999, Physical Review D, 59, 102001, arXiv:gr-qc/9710117
- Antoniadis, J., Arumugam, P., Arumugam, S., et al. 2023, Astronomy & Astrophysics, 678, A50, arXiv:2306.16214 [astro-ph]
- Babichev, E., Gorbunov, D., Ramazanov, S., Samanta, R., & Vikman, A. 2023, NANOGrav spectral index gamma=3 from melting domain walls, arXiv:2307.04582 [astro-ph, physics:hep-ph, physics:hep-th]
- Bertotti, B., Iess, L., & Tortora, P. 2003, Nature, 425, 374, number: 6956 Publisher: Nature Publishing Group
- Blasi, S., Mariotti, A., Rase, A., & Sevrin, A. 2023, Axionic domain walls at Pulsar Timing Arrays: QCD bias and particle friction, arXiv:2306.17830 [astro-ph, physics:hep-ph]
- Burrage, C., Copeland, E. J., Käding, C., & Millington, P. 2019, Physical Review D, 99, 043539, arXiv:1811.12301 [astro-ph, physics:hep-ph]
- Burrage, C., March, B., & Naik, A. P. 2023, Accurate Computation of the Screening of Scalar Fifth Forces in Galaxies, arXiv:2310.19955 [astro-ph, physics:gr-qc]
- Christiansen, Ø., Hassani, F., & Mota, D. F. 2025, Journal of Cosmology and Astroparticle Physics, 2025, 043, publisher: IOP Publishing
- Christiansen, Ø., Hassani, F., Jalilvand, M., & Mota, D. F. 2023, Journal of Cosmology and Astroparticle Physics, 2023, 009, publisher: IOP Publishing
- Christiansen, Ø., Hassani, F., & Mota, D. F. 2024, Astronomy & Astrophysics, publisher: EDP Sciences
- Clifton, T., Ferreira, P. G., Padilla, A., & Skordis, C. 2012, Physics Reports, 513, 1, arXiv:1106.2476 [astro-ph, physics:gr-qc, physics:hep-th]
- Daverio, D., Hindmarsh, M., & Bevis, N. 2016, Latfield2: A c++ library for classical lattice field theory, arXiv:1508.05610 [astro-ph, physics:hep-lat, physics:physics]
- DESI Collaboration, Adame, A. G., Aguilar, J., et al. 2024, DESI 2024 VI: Cosmological Constraints from the Measurements of Baryon Acoustic Oscillations, publication Title: arXiv e-prints ADS Bibcode: 2024arXiv240403002D
- Esposito-Farese, G. 2004, in AIP Conference Proceedings, Vol. 736, 35–52, iSSN: 0094243X arXiv:gr-qc/0409081
- Gouttenoire, Y. & Vitagliano, E. 2023, Domain wall interpretation of the PTA signal confronting black hole overproduction, arXiv:2306.17841 [astro-ph, physics:gr-qc, physics:hep-ph, physics:hep-th]
- Hinterbichler, K. & Khoury, J. 2010, Physical Review Letters, 104, 231301, arXiv: 1001.4525
- Hinterbichler, K., Khoury, J., Levy, A., & Matas, A. 2011, Physical Review D, 84, 103521
- Kibble, T. W. B. 1976, Journal of Physics A: Mathematical and General, 9, 1387 Kitajima, N., Lee, J., Murai, K., Takahashi, F., & Yin, W. 2023a, Gravitational Waves from Domain Wall Collapse, and Application to Nanohertz Signals with QCD-coupled Axions, arXiv:2306.17146 [astro-ph, physics:hep-ph]
- Kitajima, N., Lee, J., Takahashi, F., & Yin, W. 2023b, Stability of domain walls with inflationary fluctuations under potential bias, and gravitational wave signatures, arXiv:2311.14590 [astro-ph, physics:gr-qc, physics:hep-ph]
- Kovács, A., Sánchez, C., García-Bellido, J., et al. 2019, Monthly Notices of the Royal Astronomical Society, 484, 5267, arXiv:1811.07812 [astro-ph]
- Käding, C. 2023, Astronomy, 2, 128, \_eprint: 2304.05875
- Li, X.-F. 2023, Probing the high temperature symmetry breaking with gravitational waves from domain walls, arXiv:2307.03163 [astro-ph, physics:hepph]
- Llinares, C. & Brax, P. 2019, Physical Review Letters, 122, 091102, arXiv: 1807.06870

- Llinares, C. & Mota, D. 2013, Physical Review Letters, 110, 161101, arXiv: 1302.1774
- Llinares, C. & Mota, D. F. 2014, Physical Review D, 89, 084023, publisher: APS ADS Bibcode: 2014PhRvD..89h4023L
- Llinares, C. & Pogosian, L. 2014, Physical Review D, 90, 124041, publisher: APS ADS Bibcode: 2014PhRvD..90I4041L
- Lopez, A. M., Clowes, R. G., & Williger, G. M. 2024, A Big Ring on the Sky, arXiv:2402.07591 [astro-ph]
- Maiorano, M., De Paolis, F., & Nucita, A. A. 2021, Symmetry, 13, 2418, arXiv:2112.08064 [astro-ph]
- Nadathur, S. 2013, Monthly Notices of the Royal Astronomical Society, 434, 398, aDS Bibcode: 2013MNRAS.434..398N
- Peebles, P. J. E. 2023, Flat Patterns in Cosmic Structure, arXiv:2308.04245 [astro-ph]
- Perivolaropoulos, L. & Skara, F. 2022, Physical Review D, 106, 043528, publisher: American Physical Society
- Phinney, E. S. 2001, A Practical Theorem on Gravitational Wave Backgrounds, arXiv:astro-ph/0108028
- Ramazanov, S., Babichev, E., Gorbunov, D., & Vikman, A. 2022, Physical Review D, 105, 063530, arXiv:2104.13722 [astro-ph, physics:gr-qc, physics:hep-ph, physics:hep-th]
- Reardon, D. J., Zic, A., Shannon, R. M., et al. 2023, The Astrophysical Journal Letters, 951, L6, arXiv:2306.16215 [astro-ph, physics:gr-qc]
- Saikawa, K. 2017, Universe, 3, 40, \_eprint: 1703.02576
- Secrest, N., von Hausegger, S., Rameez, M., Mohayaee, R., & Sarkar, S. 2022, The Astrophysical Journal Letters, 937, L31, arXiv:2206.05624 [astro-ph, physics:gr-qc, physics:hep-ph]
- Secrest, N., von Hausegger, S., Rameez, M., et al. 2021, The Astrophysical Journal, 908, L51, arXiv: 2009.14826
- Vachaspati, T. 2007, Kinks and Domain Walls: An Introduction to Classical and Quantum Solitons (Oxford University Press)
- Vilenkin, A. 1985, Physics Reports, 121, 263
- Will, C. M. 2014, Living Reviews in Relativity, 17, 4, aDS Bibcode: 2014LRR....17....4W
- Xu, H., Chen, S., Guo, Y., et al. 2023, Research in Astronomy and Astrophysics, 23, 075024, arXiv:2306.16216 [astro-ph, physics:gr-qc]

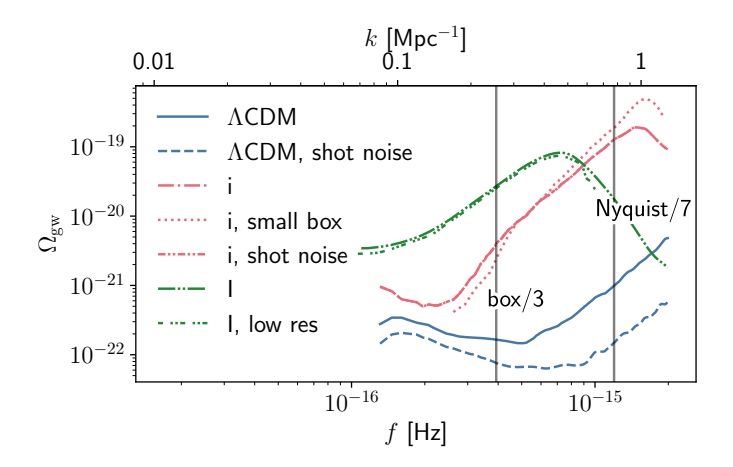


**Fig. A.1.** Numerical tests for the power spectra of gravitational waves. The red graphs are for the parameter choice, i, presented in section 3, where we used a simulation volume of (148 Mpc)<sup>3</sup>. The ΛCDM graphs in blue are using the same box volume. The graphs named 'shot noise' use 8 times as many particles. The graph 'small box' keeps the grid and particle number constant, but is using an eighth of the simulation volume, (74 Mpc)<sup>3</sup>. The green graphs are for the parameter choice I, and use a simulation volume (148 Mpc)<sup>3</sup>, but with different grid resolutions of 1280<sup>3</sup> and 512<sup>3</sup> points, respectively. The vertical lines indicate the Nyquist scale of the (148 Mpc)<sup>3</sup> boxes, and the box scale of the (74 Mpc)<sup>3</sup> box.

# **Appendix A: Numerical convergence**

In order to assess the numerical convergence of our results, we have run 4 additional simulations that we present in figure A.1 We checked that our results for the scalar field models are numerically converged by simulating the fiducial model I with a lower resolution of only 512<sup>3</sup> grids. This corresponds to the resolutions used for simulations IV-V. Figure A.1 shows perfect agreement between these two cases for the relevant range of the spectrum. Considering whether we are fully sampling the phase space, we consider the simulation i in an eighth of the box volume, keeping the number of grid points and particles fixed. We found good agreement for the overlapping resolution range, with a loss of power on large scales and a gain of power on small scales (above  $10^{-15}$  Hz) in the smaller box, as expected. One should be aware that this smaller simulation is too small to form stable domains and has the entire volume collapse into the same domain, and is therefore qualitatively different. This may explain the slightly greater slope at large frequencies. Note additionally that the two suites of simulations, I-V and i-v, shown in figure 2, cover different parameter choices and are therefore expected to be different. We tested the robustness of the obtained spectra with respect to the mass discretisation by running both the  $\Lambda$ CDM and the fiducial model i with 8 times more particles. As a result we saw that the high-frequency rise in the  $\Lambda$ CDM signal from about  $f \sim 5 \times 10^{-16} \, \text{Hz}$  is due to discretisation noise. For the scalar spectra the noise from the mass discretisation is subdominant by several orders of magnitude.

As we are simulating the sourcing of gravitational waves from domain walls, we comment now in particular on how we are resolving them. In a homogeneous background matter density,  $\rho$ , the static domain wall profile can be solved analytically, as is shown e.g. in Llinares & Pogosian (2014), giving

$$\phi(x)/v_0 = \sqrt{1 - \rho/\rho_*} \tanh\left(\frac{ax}{2L_C} \sqrt{1 - \rho/\rho_*}\right), \tag{A.1}$$

where  $v \equiv \mu/\sqrt{\lambda}$  is the vacuum expectation value of the field  $\phi$  and  $\rho_* \equiv \mu^2 M^2$  is the critical density of the phase transition. The width of the profile in conformal coordinates therefore translates to  $D \sim FL_C/\left(a\sqrt{1-\rho/\rho_*}\right)$ , where F is the thickness of the profile  $\tanh{(x/2)}$ . We can have an estimate for F from the spacing in between the two points where  $\partial_x^3 \tanh{(x/2)} = 0$ . This solves to  $x = \ln\left(2 \pm \sqrt{3}\right) \approx \pm 1.317$ , meaning that  $F \approx 2.63$ . This corresponds to a the region where the field rises to 60% of its asymptotic value. If we instead choose the region within which the field rises to 90% of its asymptotic value, we are left with  $F \approx 6$ . D is smallest in total vacuum, when  $\rho/\rho_* \to 0$ , and at the current time, when  $a \to 1$ . Since we are dealing with an inhomogeneous density distribution, the domain wall thickness will be environmentally dependent.

This means that within the steepest part, where the third derivative is positive, we will in the worst case have a resolution of  $D/dx \approx 2.63 L_C/dx$  points along the wall profile. While, for the region where the field rises to 90% of its asymptotic value, we will have  $D/dx \approx 6L_C/dx$  points. In the majority of cases, and for the majority of the time of the simulation, the ambient background density will be larger so that  $L_C/\sqrt{1-(\rho/\rho_*)^3} > L_C$ , and a < 1, in which case we will resolve more points. In our simulations, we have kept  $L_C/dx > 1$ . Simulations I and III are best and have  $L_C/dx \approx 2.6$ . For these simulations we will in the worst case have 15 points across the region where the wall rises to up to 90% of its asymptotic value. For simulation I, we also ran a lower resolution simulation, with  $L_C/dx = 1.024$ , matching the resolution of simulations IV and V, and found perfect agreement with the higher resolution run within the rising part of the power spectrum, see again figure

The spatial and temporal resolution of the dynamical and nonlinear field through the phase transition and subsequent rearrangements is complicated to establish and is handled to much more detail in the previous work of Christiansen et al. (2024), whose rules we applied here, and to which we direct the interested reader for more details.